ACS APPLIED MATERIALS & INTERFACES

Research Article

www.acsami.org

Design of Xylose-Based Semisynthetic Polyurethane Tissue Adhesives with Enhanced Bioactivity Properties

Sevgi Balcioglu,[†] Hakan Parlakpinar,[‡] Nigar Vardi,[§] Emir Baki Denkbas,[∥] Merve Goksin Karaaslan,[†] Selam Gulgen,[†] Elif Taslidere,[§] Suleyman Koytepe,[†] and Burhan Ates*[,†]

[†]Department of Chemistry, Faculty of Science, Inonu University, Malatya 44280, Turkey

[‡]Department of Pharmacology, Faculty of Medicine, Inonu University, Malatya 44280, Turkey

[§]Department of Histology-Embryology, Faculty of Medicine, Inonu University, Malatya 44280, Turkey

[∥]Department of Chemistry, Faculty of Science, Hacettepe University, Ankara 06800, Turkey

Supporting Information

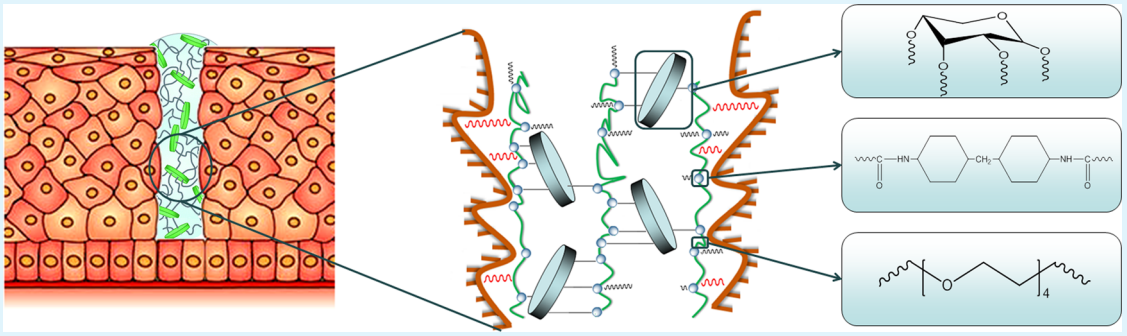

ABSTRACT: Developing biocompatible tissue adhesives with high adhesion properties is a highly desired goal of the tissue engineering due to adverse effects of the sutures. Therefore, our work involves synthesis, characterization, adhesion properties, protein adsorption, *in vitro* biodegradation, *in vitro* and *in vivo* biocompatibility properties of xylose-based semisynthetic polyurethane (NPU-PEG-X) bioadhesives. Xylose-based semisynthetic polyurethanes were developed by the reaction among 4,4′-methylenebis(cyclohexyl isocyanate) (MCI), xylose and polyethylene glycol 200 (PEG). Synthesized polyurethanes (PUs) showed good thermal stability and high adhesion strength. The highest values in adhesion strength were measured as 415.0 ± 48.8 and 94.0 ± 2.8 kPa for aluminum substrate and muscle tissue in 15% xylose containing PUs (NPU-PEG-X-15%), respectively. The biodegradation of NPU-PEG-X-15% was also determined as 19.96 ± 1.04% after 8 weeks of incubation. Relative cell viability of xylose containing PU was above 86%. Moreover, 10% xylose containing NPU-PEG-X (NPU-PEG-X-10%) sample has favorable tissue response, and inflammatory reaction between 1 and 6 weeks implantation period. With high adhesiveness and biocompatibility properties, NPU-PEG-X can be used in the medical field as supporting materials for preventing the fluid leakage after abdominal surgery or wound closure.

KEYWORDS: *xylose, polyurethane, tissue adhesive, biocompatibility, semisynthetic materials*

INTRODUCTION

A problem increasing day by day is that millions of people suffer from wounds including skin wounds, surgical or traumatic disruption, intestine, connective tissue, muscles, tendons and membranes that require closure.[1,2] Although, suture is still the main device to close the wounds, it has some disadvantages such as granuloma formation, nerve damage, leakages, inflammatory reactions, requiring anesthesia and scar formation.[3,4] Therefore, tissue adhesives have been good alternatives as supporting materials.[5] This fact is based on their attractive properties including reduction of surgery time, mitigation of infection, preventing leakages, easy application, no removal requirements, less pain and great cosmetic results.[6−8] Because of these characteristics of tissue adhesives, especially in preventing leakages and acceleration of wound healing, they can be used single or combined with sutures. Despite these advantages, the currently available tissue adhesives still have significant limitations and drawbacks such as low tensile strength, biocompatibility and expensiveness.[4]

Surgical adhesives can be divided as biological, synthetic, semisynthetic and biomimetic.[9−14] Among the synthetic or semisynthetic bioadhesives, polyurethanes have been considered as a promising adhesive material due to their biocompatibility and biodegradability properties.[4,6] UV curable polyurethane adhesive based on polycaprolactone diol and 2-isocyanatoethyl methacrylate was developed by Ferreira et al.

Received: December 16, 2015
Accepted: January 29, 2016
Published: January 29, 2016

DOI: 10.1021/acsami.5b12279
ACS Appl. Mater. Interfaces 2016, 8, 4456−4466

According to their results, biodegradability was around 10% after 6 weeks and material is slightly hemolytic.[15] In the another study, Ferreira et al. developed a biodegradable urethane-based bioadhesive containing free isocyanate groups. In that research, castor oil hydroxyl groups were modified with isophorone diisocyanate. Hemolysis tests showed that the urethanes presented a nonhemolytic character.[6]

In this study, semisynthetic polyurethane bioadhesives were designed from the natural saccharide-based monomers for surgical operations. We synthesized these polyurethanes from nonaromatic and totally biocompatible monomer structures. Nonaromatic monomer units were chosen as xylose for high cross-linking, 4,4′-methylenebis(cyclohexyl isocyanate (MCI) for enhancing biocompatibility and PEG groups for flexibility and processability. These monomer compositions determine most of the properties of adhesive such as adhesion, mechanical properties, biocompatibility, biodegradability and toxicity of the degradation products. In this polyurethane, xylose provides four hydroxyl group and a formyl functional group on the polymer chain structure, as suitable adhesive for tissue structure. Thanks to hydroxyl units, it may form hydrogen bond between polymer chains and tissue-to-tissue interfaces. Another important group is also MCI units in the structure of the synthesized polyurethane as diisocyanate. Especially, this unit provides conformational flexibility, biocompatibility and mechanical strength. In addition, injectable polyurethanes in body conditions were obtained from adjusting the ratio and molecular structure of PEG units. The synthesized polyurethanes were subsequently characterized by Fourier transform infrared spectroscopy (FT-IR), dynamic contact angle measurement, atomic force microscopy (AFM) and thermal analysis techniques. In addition, adhesive properties, biodegrability, protein adsorption, *in vitro* cytotoxicity and *in vivo* biocompatibility of the polyurethanes were studied in detail.

EXPERIMENTAL SECTION

Materials. 4,4′-Methylenebis(cyclohexyl isocyanate) (MCI) was ordered from Fluka and dried in 4 Å molecular sieves before the experiment. Sodium dodecyl sulfate, o-phthaladehyde, tetrahydrofuran (THF), trimethylamine, hexadecyl trimethylammonium bromide (HETAB), ethanol and KBr were supplied from Merck. THF was also dried by vacuum distillation. Dimethyl sulfoxide (DMSO) and dimethylformamide (DMF) were obtained from Carlo Erba. 3-(4,5-dimethylthiazol-2-yl)-2,5-diphenyltetrazolium bromide (MTT) was purchased from AppliChem. Other chemicals were ordered from Sigma-Aldrich. All reagents were used as received without any further purification. All other reagents used in this study were analytical grade.

Synthesis of NPU-PEG-X Polyurethanes. In this study, solution polymerization techniques were applied in the synthesis of all polymers. Xylose-based polymers (NPU-PEG-Xs) were produced with MCI, xylose and PEG200 via polycondensation using THF:DMF (9:1) as a solvent and triethylamine as a catalyst. NPU-PEG polymers were also produced using exactly the same procedure without xylose. The molar ratios based on functional groups of MCI:xylose:PEG200 units in the PUs were 1:0:1, 1:0.05:0.95, 1:0.1:0.9 and 1:0.15:0.85, respectively. These materials were referred as NPU-PEG, NPU-PEG-X-5%, NPU-PEG-10% and NPU-PEG-X-15%, respectively. First, MCI was dissolved in THF:DMF mixture. Then, PEG200 and xylose were added to the isocyanate solution at the previous rates. Different weight ratios of NPU/PEG/X were prepared and reacted with 0.1 wt % triethylamine under nitrogen atmosphere with mechanical stirring at 90 °C for 8 h. After cooling to room temperature, the resulting PUs were obtained by removing of the solvent under vacuum. The PUs were washed several times with ether for further use.

The reactions were followed with FT-IR. During the following reactions, disappearance of the characteristic isocyanate peak at 2265 cm^{-1} was used to determine whether the reaction was terminated. It was observed that the peak decreased in time and the reactions were terminated when the peak disappeared.

Physicochemical Property Analysis. The structure of the PUs was characterized by FT-IR. FT-IR was recorded on a PerkinElmer 283 spectrum in the wavelength range of 400−4000 cm^{-1}.

Thermal behavior of the PUs was investigated precisely with thermogravimetric analysis (Shimadzu 50) (TGA), differential thermal analysis (Shimadzu 50) (DTA) and differential scanning calorimetry (Shimadzu 60) (DSC). Thermal stability was determined by TGA and DTA analysis in air atmosphere and glass transition temperature (T_g) was determined by DSC. The analyses were carried out at a heating rate of 5 °C/min under nitrogen atmosphere from 20 to 800 °C using 10 mg for TGA and DTA, and 5 mg for DSC of each sample. For DSC analysis, nitrogen was used as the purge gas with a flow rate of 40 mL/min.

The hydrophilicity of NPU-PEG-Xs was determined by dynamic contact angle measurement. In order to measure of dynamic contact angle, one part of the polyurethane solution was degassed in a vacuum and then quickly transferred to a glass plate using a doctor blade (e = 2 mm). The solvent was evaporated at 100 °C for 3 h. The film was removed from the glass plate by soaking it in cold water. These films were transparent, homogene and flexible. During the analyses SEO Phoenix-300 Automatic device was used and analyses were performed using a Wilhelmy plate technique.

Atomic force microscopy (AFM) measurements were performed on film prepared from NPU-PEG-X-15% using XE-100E (Park Systems Corp., Suwon, Korea) in noncontact mode by NSC36/Cr−Au type cantilevers with 0.5 Hz scanning speed. AFM measurements were carried out at two different times as before and after adhesion tests. In order to prepare PU films, NPU-PEG-X-15% were solved in ethanol (2:1, w/v) and transferred to the aluminum substrate and dried in incubator at 37 °C. These prepared films were used for AFM images of NPU-PEG-X-15% before adhesive performance tests. The AFM measurements were carried out under moisture controlled medium in ambient conditions (22 ± 2 °C). Next, adhesion test were applied NPU-PEG-X-15% by using aluminum substrates for 1 h curing time and the AFM measurements were performed again. The surface properties and topographies of the PUs were compared with the before and after the adhesion test.

Adhesion Strength Analysis. Adhesion strengths tests of NPU-PEG-Xs were performed using aluminum substrats (2 cm width x 5 cm length) and muscle tissue. The aluminum substrats were polished by grinding well and were cleaned after polishing by soaking for 10 min each in ethanol and then water. The aluminum substrats were dried overnight in air at room temperature. A 20 mm × 20 mm (4 cm^2) overlap area was used with 0.2 g adhesive samples dissolved in 50 μL of absolute ethanol. After overlap, samples were incubated for 1 and 24 h cure at room temperature. Furthermore, adhesive strength tests of NPU-PEG-Xs were performed using fresh muscle tissue for 24 h curing time at room temperature. Fresh muscle tissues were fixed on dried aluminum substrats (2 cm × 2 cm) using a commercial cyanoacrylate glue. 0.2 g of NPU-PEG-Xs dissolved in 50 μL of absolute ethanol were used for adhesion of overlap area. Bonding surface of muscle tissues was the moist when NPU-PEG-Xs were applied. After curing times, shear load-extension curves were obtained with material strength testing machine (SYC-500, Sundoo, China). The force applied to the fixture was measured with a 500 N load cell. Samples were held in place in the testing and extended in the shear direction at a speed of 40 mm/min. Adhesion force, in Newtons, was determined by the maximum point of the distance versus force plot, just prior to failure, after which the force dropped substantially. Adhesion forces expressed in Pascals (Pa) were obtained by dividing the shear force (in Newtons) by the adherend over lap area (in m^2). Each adhesion measurement was repeated at least five times. Results were given as the mean ± standard deviation.

***In Vitro* Biodegradation Analysis.** Biodegradation studies were carried out according to the ASTM method F1635-04. Samples were prepared as 1 cm diameter discs for the experiments. The starting mass of the samples was 0.1 g. The degradation rates were determined from

DOI: 10.1021/acsami.5b12279
ACS Appl. Mater. Interfaces 2016, 8, 4456−4466

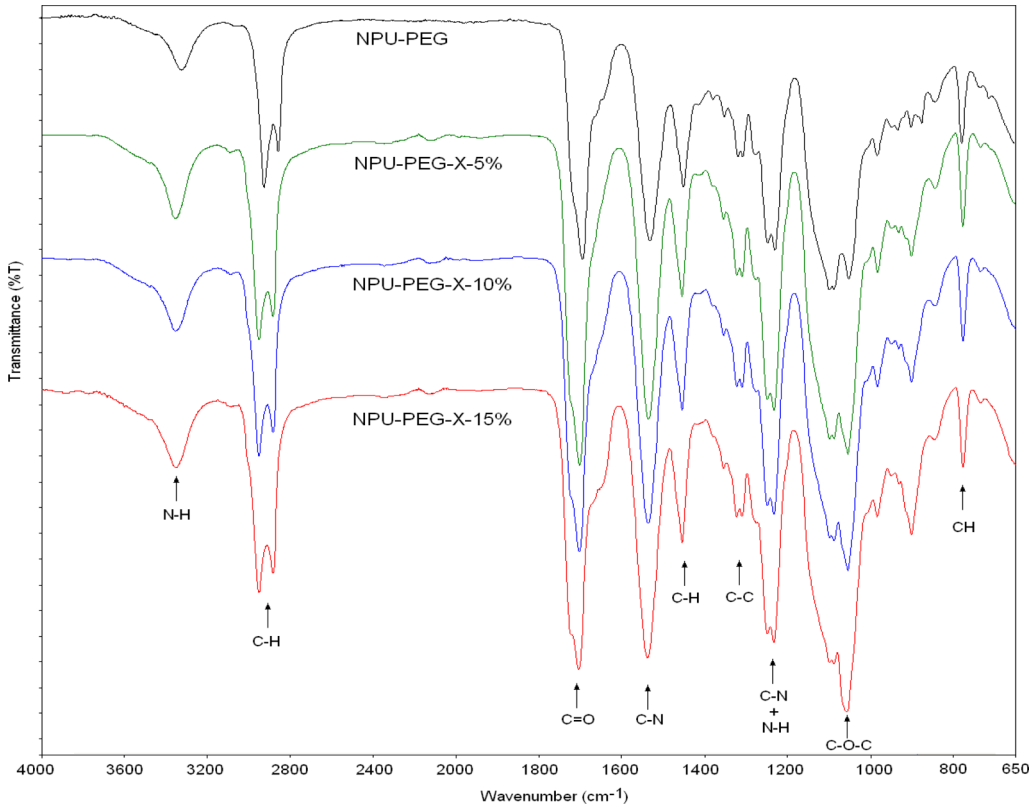

Figure 1. FT-IR spectra of NPU-PEG and NPU-PEG-Xs.

the weight loss of the PUs. In the experiment, samples were immersed in a 50 mM phosphate buffer solution (PBS, pH 7.4) at 37 °C. At predetermined time intervals (1, 2, 3, 4, 6 and 8 weeks), the samples were taken out, washed with distilled water and dried at room temperature for 2 days. Experiments were performed three repetitions for each sample. Weight loss was calculated with the following equation:

$$\text{weight loss}\ (\%) = 100 \times [1 - (W_t/W_0)]$$

where W_0 and W_t are the dry sample weight before and after degradation, respectively.

In addition, degradation processes were followed by FT-IR at 0, 4 and 8 weeks. To observe the degradation type, SEM images of NPU-PEG-X-10% were also scanned at 0 and eighth weeks.

Protein Adsorption Analysis. Protein adsorption tests were performed according to the standard protocol[7] with bovine serum albumin (BSA) and fibrinogen proteins. For the protein adsorption test, polymers were weighed 0.1 g and prepared using 1 cm diameter discs. The prepared discs were first washed with PBS for 1 h and then were immersed in 5 mL of BSA (0.32 μg/mL) or fibrinogen (0.03 μg/mL) solution at 37 °C. Incubation times were 16 and 3 h for BSA and fibrinogen solution, respectively. After this incubation, samples were removed from the protein solution and were washed twice with PBS. Then, to remove adsorbed protein from NPU-PEG-Xs the discs were immersed in 1 mL of 1% sodium dodecyl sulfate (SDS)-water solution for 3 h followed by ultrasonication for 5 min. Amount of the protein in the SDS solution was determined by the *o*-phthaldehyde (OPA) fluorospectrometric protein assay protocol. Results are given as μg protein/cm^2 for film area. All measurements were performed at least three repetitions and results were statistically analyzed by using GraphPad Prism 5.0 program.

Cytotoxicity Analysis by MTT Assay. MTT assay was used to test the cytotoxicity of the PUs (ISO 10993-5). For the experiments, 0.2 g of PUs was placed into a sterile falcon tube. Then, 1 mL of absolute ethanol was added to each tube followed by sterilization under UV light for 1 h. Excess alcohol on the PUs was evaporated, and samples were washed several times with sterile PBS (pH 7.4). For the cytotoxicity assay, fresh cell culture media (MEM medium; containing 10% FCS and 1% L-glutamine) was added into the sample tubes. Samples were incubated with medium for 72 h at 37 °C. While the samples were being incubated, rat aortic endothelial cells (RAOEC) were seeded into 96-well plates at a density of 2 × 10^{3}cells/well in 1 mL cell culture medium and allowed to attach for 24 h at 37 °C under 5% CO_2 environment. At the end of the incubation time, culture media was discarded and replaced by medium, incubated with samples as 100 μL/well. Fresh medium was used as control and all samples were incubated at 37 °C for 24 h. 100 μL of fresh medium containing 1% MTT (5 mg/mL, in PBS, pH 7.4) was pipetted to the wells. After 4 h, medium was aspirated and 100 μL of DMSO was pipetted to dissolve formazan crystals. Afterward, the optical density was read on an ELISA reader at 570 nm on the basis of linear absorbance to the number of living cells in the culture.

Preliminary Animal Study For *In Vivo* Biocompatibility Analysis. NPU-PEG-X-10% was used in animal studies for *in vivo* biocompatibility test. Twenty-four adult male of Wistar rats were divided into four groups (n: 6) as Group 1: Control (1 week), Group 2: NPU-PEG-X-10% (1 week), Group 3: Control (6 weeks) and Group 4: NPU-PEG-X-10% (6 weeks). For experimental groups, NPU-PEG-X-10% samples were weighed as 0.2 g discs, and were sterilized by UV light for 1 h. During the surgical procedure, rats were anesthetized and the samples were implanted subcutaneously in the dorsal area of animals.[8,17] PP (polypropylene) materials were applied in the control group of animals. At the end of the application time, to determine acute (1 week) and chronic (6 weeks) effects, surrounding muscle tissue was removed and histological and biochemical inflammation parameters were determined.

Histological Evaluation. For histological evaluation, surrounding tissues of the material were taken and divided into 3−4 mm parts in size. Subsequently, the tissues were fixed in 10% formaldehyde for 24 h followed by placing into the plastic tissue cassettes. After the fixation, the tissues were washed in running tap water for 24 h and then were dehydrated in alcohol and embedded in paraffin followed by making pellucid blocks with xylene. Five micron sections were taken from

DOI: 10.1021/acsami.5b12279
ACS Appl. Mater. Interfaces 2016, 8, 4456−4466

paraffin blocks by Leica RM2145 microtome. To observe the general histological structure hematoxylin-eosin staining method, to distinguish macrophages PAS (Periodic Acid Schiff) staining method, to distinguish mast cells methyl green pyronin staining method and to investigate the collagen density Masson's trichrome staining method were applied to the sections. In the tissues which were around the material, a 0−3 scoring was made by evaluating neutrophil, lymphocyte and macrophage infiltration, the density of mast cells and collagen in the connective tissue. They were grouped as Score 0: normal, Score 1: mild (0−25% damage), Score 2: moderate (25−75% damage), Score 3: severe (>75% damage).[18] The specimens were examined and scored by Leica DFC280 light microscopy and Leica Q (Leica Micros Imaging solution Ltd., Cambridge, UK) image analysis system and their photos were taken.

Biochemical Evaluation. Myeloperoxidase (MPO) activity and nitrite oxide (NO) levels were determined in the tissue samples as biochemical inflammation parameters.

Myeloperoxidase (MPO) Activity. Samples were weighed 0.1 g and put into 1 mL of phosphate buffer (50 mM, pH 6) and all tissues were homogenized under ice with a IKA-Werke T25 homogenizer. Then, homogenates were centrifuged with Hettich Universal 320 microcentrifuge at 15000 G for 15 min at 4 °C. The pellets were separated from the supernatant and added 500 μL of HETAB solution (0.5% w/w in 50 mM, pH 6 phosphate buffer). The solutions were allowed freezing-thawing twice and sonication for 15 s (Sonics VCX130). Then, samples were centrifuged at 15000 G for 15 min. 25 μL of supernatant and 200 μL of reaction mixture were added into 96-well plates and the measurement was performed at a wavelength of 460 nm with BioTek Eon Eliza microplate reader. MPO activity results were given in unit per gram of wet tissue.

Nitric Oxide (NO) Assay. 0.1 g of muscle tissue was homogenized and was sonified with an ultrasonifier by three cycles (20 s sonications with a 30 s pause) in 5 volumes ice-cold PBS (pH 7.4). Supernatant was obtained after centrifuge (15000*g*, 10 min, 4 °C) and was subjected to NO assay, immediately. Nitric oxide levels were determined by colorimetric method using Cayman Nitrite/Nitrate Assay Kit based on Griess reaction. The Griess reaction is summarized as the azo coupling between diazonium species, which are produced from sulfanilamide with NO_2, and naphthylethylenediamine. After reaction, azo product was measured at 540 nm by using a BioTek Eon Eliza microplate reader. NO levels were given in nmol/g of tissue.

Statistical Analysis. The one-way analysis of variance (ANOVA) and Tukey's multiple comparison tests were used to analyze the significance of the differences between the experimental groups. Results were considered to be significant when $p < 0.05$.

RESULTS AND DISCUSSION

Synthesized NPU-PEG-Xs with different monomer weight ratios were characterized by FT-IR, DSC, DTA, TGA, contact angle, adhesion strength, AFM measurement, biodegradation, protein adsorption, *in vitro* cytotoxicity and *in vivo* biocompatibility.

Chemical Characterization. Chemical structures of PUs were confirmed by FT-IR spectroscopy. Figure 1 shows the FT-IR spectrum of NPU-PEG and xylose-based PUs (NPU-PEG-Xs). In the FT-IR spectra of NPU-PEG and NPU-PEG-Xs, there is no free isocyanate peak at 2265 cm^{-1} and this indicates that there is no residual MCI in the polymer structure. A characteristic FT-IR peak is observed at 1733 cm^{-1}, which is belong to −C═O ester groups in the NPU-PEG-Xs. In the FT-IR spectrum, the −C—H stretching frequencies for the aliphatic $-CH_2-$ groups are relatively weak and observed at ∼2927−2890 cm^{-1}. The peak at 3300 cm^{-1} is ascribed to the N—H stretching frequency. Moreover, the peaks at 1522 cm^{-1} belong to −N—H and −C—H stretching vibrations. These results also indicate that both NPU-PEG and xylose-based PUs were synthesized successfully. Increasing xylose ratio in the PUs increases aliphatic −CH stretching vibration. Thus, excessive branching and cross-linking also leads to a loss of film flexibility.

Thermal Properties. To investigate the structural and stability effect of xylose, MCI and PEG units, thermal analysis such as TGA, DTA and DSC were performed. First, the thermal stabilities and thermal degradation properties of the xylose-containing PUs were examined via TGA. Figure 2 shows

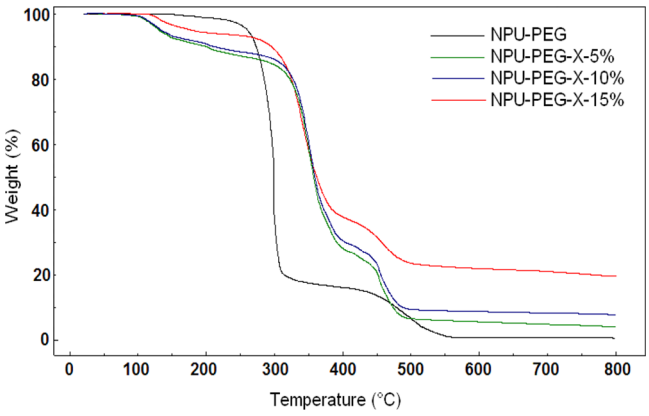

Figure 2. TGA thermograms of NPU-PEG and NPU-PEG-Xs.

the comparison of TG curves depending on xylose ratios of PUs. Three thermal degradation patterns were observed in TGA thermograms of xylose containing PUs. The first thermal degradation of the NPU-PEG-Xs resulted from the degradation of xylose units. Second thermal decomposition was observed corresponding to the degradation of the soft segment of PEG and $-CH_2$ groups of isocyanate units. The last thermal degradation pattern resulting from the hard segment of cyclic $-CH_2$ groups of isocyanate units was observed as the last thermal decomposition. All the thermal decompositions are range from 150 to 300, 300−375 and 380−450 °C in the thermograms, respectively. As expected, the thermal decomposition of NPU-PEG polymer was characterized with two distinctive steps, which correspond to the degradation of hard and soft segments in polyurethane structure. These two thermal degradation patterns were observed resulting from the PEG and MCI units in the PUs. These results are correlated with thermal degradation curves of other saccharide-based polyurethanes.[19] The initial decomposition temperature and percentage of the residue at 600 °C are higher in NPU-PEG-X-5% compared to NPU-PEG-X-10% or NPU-PEG-X-15%. In Figure 2, the thermal stability of PUs increased as parallel with molar ratios of xylose. In addition to, with increasing xylose concentration, the flexibility of PU chains is decreased due to the excessive branching and cross-linking. The structure of NPU-PEG was linear and generally quite packed. This structure had also low free volume and high "initial decomposition temperature". NPU-PEG showed low char yield (∼3.2%). When compared to NPU-PEG, char yield of the xylose-based polyurethanes increased with increasing the amount of xylose. In TGA analysis, char yields of NPU-PEG-X-5%, NPU-PEG-X-10% and NPU-PEG-X-15% at 600 °C were 5.2%, 9.4% and 21.8%, respectively. These data proved an increase in the thermal stability of the structure by being increased the amount of xylose. As a result, all the prepared xylose-based polyurethanes may suitable for usage in medical tissue adhesive application in term of high thermal stability.[20]

DOI: 10.1021/acsami.5b12279
ACS Appl. Mater. Interfaces 2016, 8, 4456−4466

Thermal behaviors of PUs were also investigated by DTA analysis and results were matched with TG analysis. Figure 3

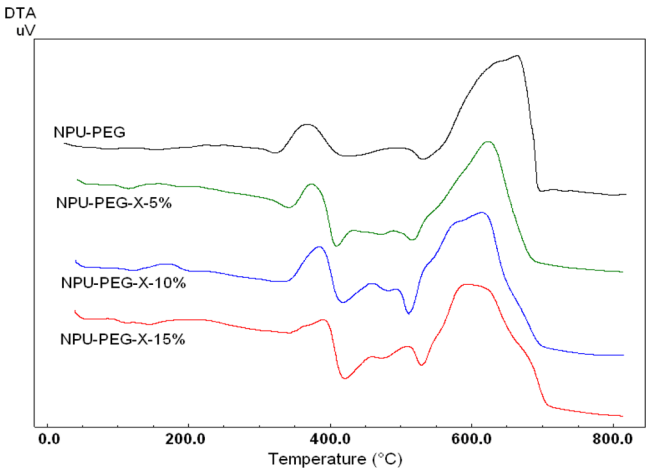

Figure 3. DTA thermograms of NPU-PEG and NPU-PEG-Xs.

shows the DTA thermograms of NPU-PEG, NPU-PEG-X-5%, NPU-PEG-X-10% and NPU-PEG-X-15%. All thermograms of the xylose containing PUs include four thermal decomposition peak (first peak at about 150−310 °C belongs to − CH_2 groups of PEG, second peak at 310−380 °C belongs to cross-linking of xylose, third peak at 400−500 °C belongs to bridge CH_2 groups of isocyanate and last peak at ∼500 °C belongs to cyclic CH_2 groups of isocyanate). However, in the DTA thermogram of NPU-PEG, three peaks were observed as different from xylose containing PUs due to lineer structure. The thermal stability of the polymers was increased by being increased of xylose content due to the cross-linking of polymer chains. DTA measurement results are compatible with the TGA results.

Figure 4 shows DSC thermograms of NPU-PEG and xylose-based PUs samples. The T_g of the NPU-PEG was observed at

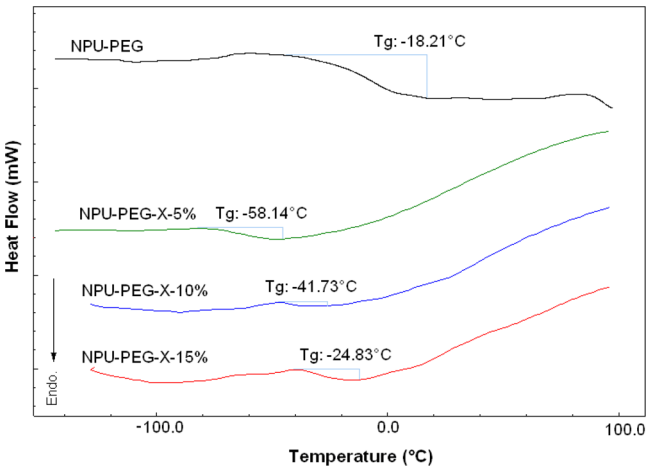

Figure 4. DSC thermograms of NPU-PEG and NPU-PEG-Xs.

around −18.21 °C and is higher than NPU-PEG-Xs. NPU-PEG has linear polymer chain structure. Thus, it forms a stacked polymer chain structure more compact than NPU-PEG-Xs. Crystallinity and cross-link degree are two important parameters that affect the T_g of the polymers. In general, increasing crystallinity and/or cross-linking in a polymer structure cause an increase in T_g.[21] Intermolecular forces and crystallinity are strong when the polymer chains pack together in a regular way as in these linear polyurethanes. Therefore, T_g of this stacked structure increases. On the other hand, T_g values of PU-PEG-Xs increased with the xylose ratio of the polyurethanes. The T_g values of PU−PEG-X-5%, PU-PEG-X-10% and PU-PEG-X-15% were observed as −58.14, −41.73 and −24.83 °C, respectively. The T_g increased steadily with the xylose content for all three types of PUs. The incorporation of xylose into the PU structure leads to an increase in cross-link density. The high cross-link density restricted main chain motion and caused an increase in T_g.

Contact Angle Measurements. Contact angle is an indicator of surface heterogeneity, roughness, permeation of the water into the material and/or extending to which the material surface reorients the drop. To determine the hydrophilicity of PUs, dynamic contact angle measurements were determined using Wilhelmy plate technique.[22] Contact angle results were obtained at 51.23 ± 1.46, 55.90 ± 3.06, 58.91 ± 1.47 and 62.19 ± 3.34° for NPU-PEG, NPU-PEG-X-5%, NPU-PEG-X-10% and NPU-PEG-X-15%, respectively (Table 1). Xylose ratio in polyurethane structure increased the contact

Table 1. Water Contact Angles on the Surfaces of NPU-PEG and NPU-PEG-Xs

sample name	contact angle (deg)
NPU-PEG	51.23 ± 1.46
NPU-PEG-X-5%	55.90 ± 3.06
NPU-PEG-X-10%	58.91 ± 1.47
NPU-PEG-X-15%	62.19 ± 3.34

angle and decreased the hydrophilicity. However, changes in the contact angle of samples were not in very large scales. In addition, NPU-PEG and NPU-PEG-Xs have wettable surface structure so they show high biodegradability.

Adhesion Strength Properties. Adhesive properties of the xylose-based PUs were determined using lap shear adhesion test in accordance with ASTM (F2255-03, "Test Method for Strength Properties of Tissue Adhesives in Lap-Shear by Tension Loading") standards.[23−25] Adhesion test results for 1 and 24 h and shear load-extension curves for 24 h of PUs were given in Figure 5. Adhesion strength values of NPU-PEG-X-5%, NPU-PEG-X-10% and NPU-PEG-X-15% were 79.6 ± 36.9,

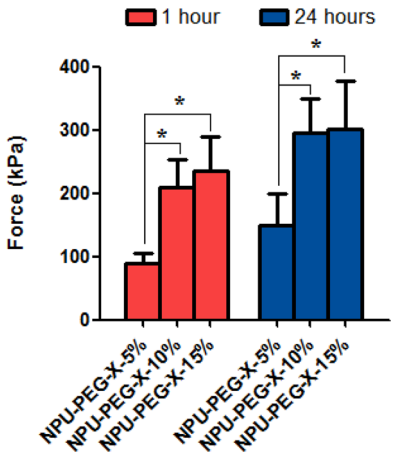

Figure 5. Adhesive strengths of PUs under various time conditions. Data are expressed as mean SD (n = 5). * Significantly different from NPU-PEG-X-5%, (p < 0.05).

DOI: 10.1021/acsami.5b12279
ACS Appl. Mater. Interfaces 2016, 8, 4456−4466

232.6 ± 52.0, 330.0 ± 10.4 for 1 h and 189.6 ± 23.4, 382.3 ± 16.9, 415.0 ± 48.8 for 24 h, respectively. Furthermore, adhesion strengths statistically showed an increase ($p < 0.05$) in the NPU-PEG-X-10% and NPU-PEG-X-15% compared with the NPU-PEG-X-5% for 1 and 24 h curing times. Adhesion strength increased with cross-linking ratio of polyurethane as parallel with literature.[26−30]

In previous studies, for chlorogenic acid (CLA)-based polyurethanes, the highest adhesion values were measured as 226.6 ± 35.2 kPa and 373.3 ± 47.5 kPa for 1 and 24 h curing times in 10% of CLA containing PUs, respectively.[9] According to our adhesion test results, NPU-PEG-X-15% polymer showed higher values than CLA-based PUs.

We also tested adhesive strength of NPU-PEG-X samples for muscle tissue (Figure 6). For 24 h curing times, in parallel with the concentration of xylose in PUs, adhesive strength values were identified as 46.2 ± 25.2, 52.2 ± 24.0 and 94.0 ± 2.8 kPa, respectively. In addition, adhesion strengths statistically showed an increase ($p < 0.05$) in the NPU-PEG-X-15%, as compared with the NPU-PEG-X-10% and NPU-PEG-X-5%. In previous studies, gelatin, chitosan and fibrin-based adhesives were measured at 12−20, 3 and 0.7−27 kPa as adhesive strength after 24 h of curing, respectively.[31−33] Especially, fibrin glue is used quite often in surgical operations.[7] According to our test results, adhesion strength of NPU-PEG-Xs is very high compared with the mentioned adhesives. Therefore, NPU-PEG-Xs may find the area of application as medical tissue adhesive.

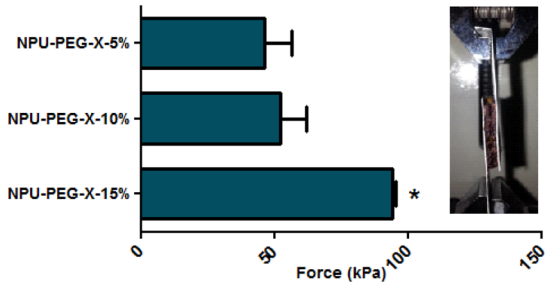

Figure 6. Actual image of lap shear testing using muscle tissue surfaces (on the right side) and adhesive strengths of PUs (on the left side). * Significantly different from NPU-PEG-X-15% vs NPU-PEG-X-10% and NPU-PEG-X-5%, ($p < 0.05$).

AFM Images. AFM is the best method for investigating the surface topography of the adhesive samples with high resolution. Thus, before and after the adhesion test of NPU-PEG-X adhesive materials, the surface morphologies were investigated by AFM in noncontact mode using standard noncontact cantilever with silicone tips. AFM images were shown in Figure 7 with 3D.

Figure 7 shows surface topology of the adhesive material before (A) and after (B) adhesive performance tests (shear test). Uniform covering of adhesives on the surface of aluminum metals is very important for its adhesive performance in order to get equal adhesion strength in all directions. Therefore, before adhesive performance test, the AFM measurements of NPU-PEG-X-15% were carried out and the surface topology of untreated adhesive material was seen as flat, smooth and homogeneous (Figure 7A). However, after the shear test, fibers and local adhesion zones were seen on the adhesive material (Figure 7B). During the measurement of

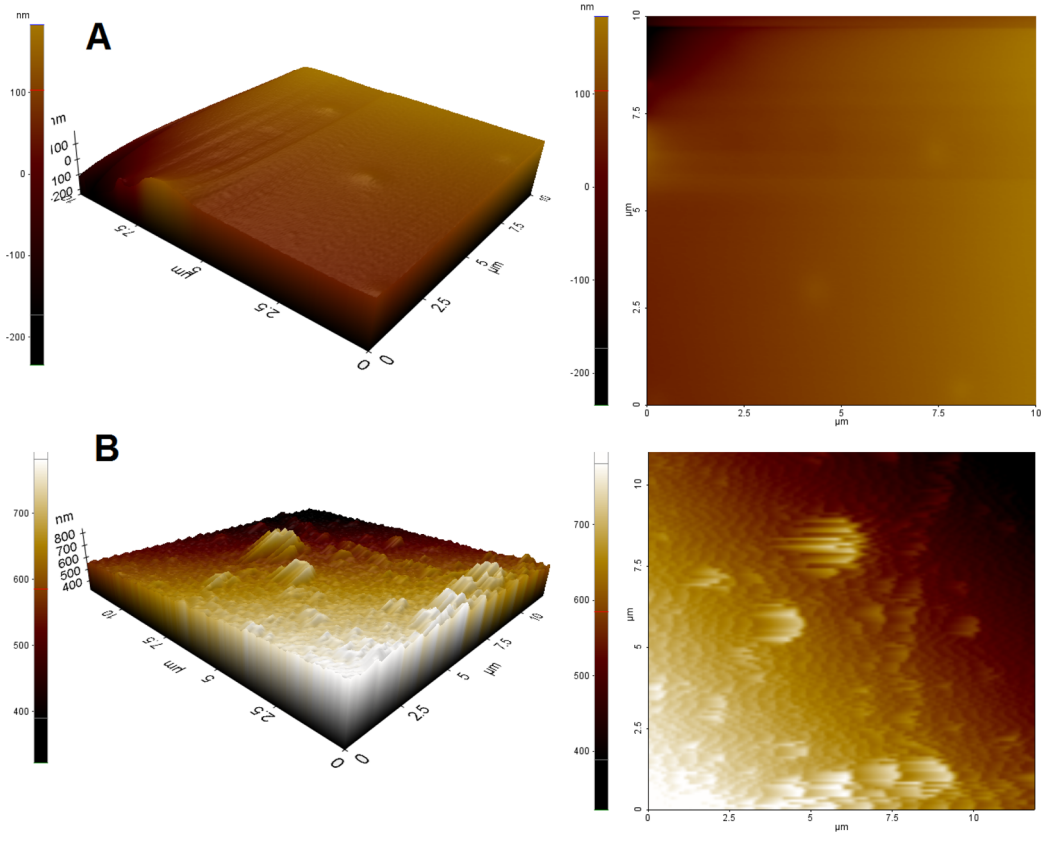

Figure 7. AFM images of NPU-PEG-X-15% before (A) and after (B) adhesive performance tests (shear test).

DOI: 10.1021/acsami.5b12279
ACS Appl. Mater. Interfaces 2016, 8, 4456−4466

adhesion properties, the surface properties and topographies of the sample was changed and surface topology of NPU-PEG-X-15% was shown as quite fractal, rough and fibrillary structure.

***In Vitro* Biodegradation Properties.** Figure 8 illustrates the weight loss of PUs during 8 weeks incubation time. The highest value was 19.96 ± 1.04 in NPU-PEG-X-15% for 8 weeks incubation. Bulk degradations of all PUs were also determined from FT-IR spectrum (Figure S1) and SEM images (Figure 9). Generally, for all PUs three degradations were observed resulting from hard segments (isocyanate groups), soft segments (PEG groups) and cross-linking groups (xylose) (Figure S1). Because of the degradation of CH_2 groups in isocyanate units, −COOH groups are formed and thus we can observe an expansion in −OH stretching vibration at 3300−3650 cm^{-1} in FT-IR spectra. Furthermore, there are no NH_2 and isocyanate groups in FT-IR spectra during degradations so we can say that toxic groups were not formed. In addition, at 1276 cm^{-1}, we can observe a decrease in −CO stretching vibration originated from degradation of xylose units. Obviously, when PUs are compared with each other, the percentage weight loss in PUs was increased with increasing in the percentage of xylose. According to SEM images, biodegradation of NPU-PEG-Xs was clearly seen after 8 weeks of incubation period (Figure 9).

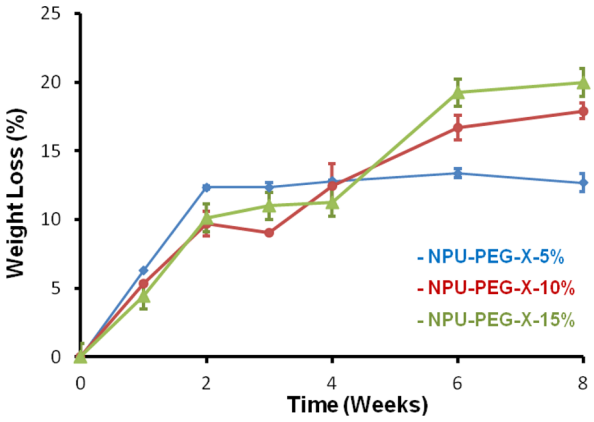

Figure 8. Biodegradation profile of NPU-PEG-Xs versus time.

Protein Adsorption Properties. Protein adsorption results were separately shown as BSA and fibrinogen adsorption. BSA, the most abundant protein in plasma, is a very significant protein in terms of protein adsorption properties of biomaterials.[34,35] Hence, we measured the adsorption of BSA on NPU-PEG-X polymer surfaces to investigate protein resistance. Figure 10 shows BSA adsorption on NPU-PEG-X surfaces. The amounts of adsorbed BSA were 8.06 ± 0.95, 11.99 ± 2.24 and 15.44 ± 2.48 $\mu g/cm^2$ for NPU-PEG-X-5%, NPU-PEG-X-10% and NPU-PEG-X-15%, respectively. According to the results, it is so clear that the increase in BSA adsorption is statistically significant ($p < 0.05$) with increasing the concentration of xylose in PUs. The reason for this was that the porous polymer structure was formed due to increased branching in the polymer with increasing xylose ratio. In the previous studies, BSA adsorptions of pMEMA poly(2-methoxyethyl methacrylate), pHEMA poly(2-hydroxyethyl methacrylate), pAAm poly(acrylamide), pMMA poly(methyl methacrylate) and pSt poly(styrene) polymers were measured as 1.5, 4.7, 5.7, 9.2 and 13.0 $\mu g/cm^2$, respectively.[36] BSA

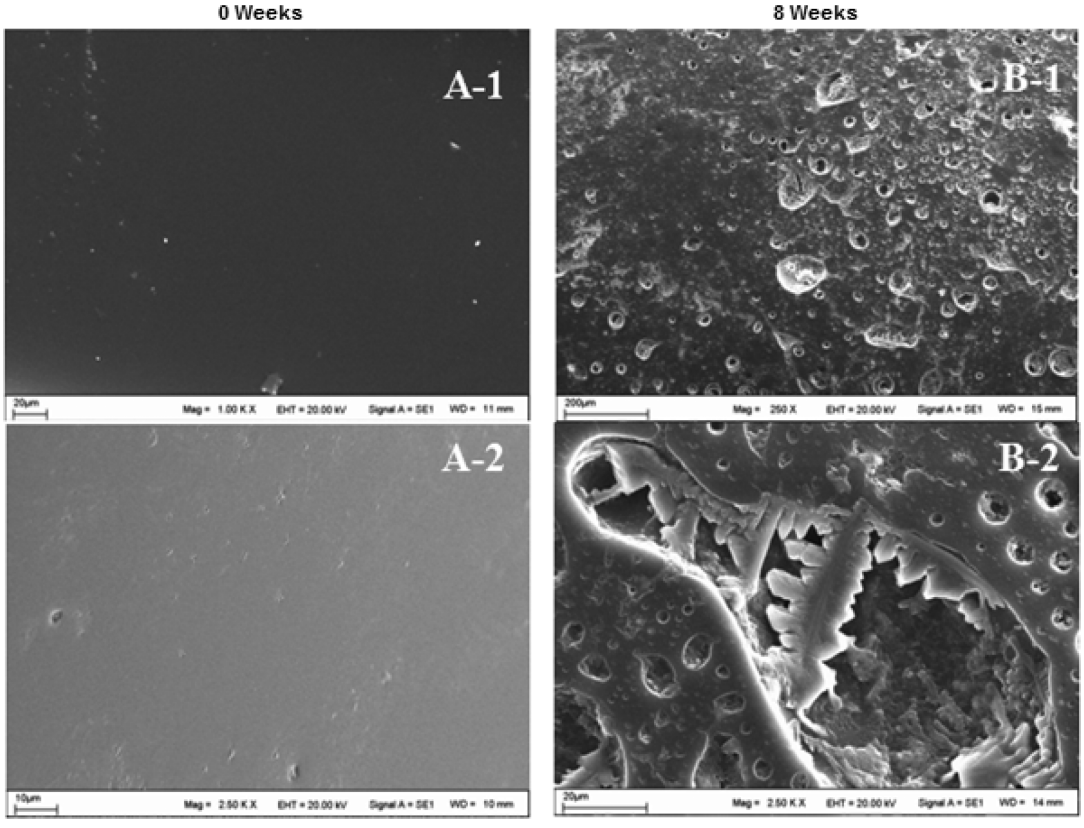

Figure 9. SEM images of the biodegradation process of NPU-PEG-Xs (A) at the beginning, (B) at the end of the 8 weeks.

DOI: 10.1021/acsami.5b12279
ACS Appl. Mater. Interfaces 2016, 8, 4456−4466

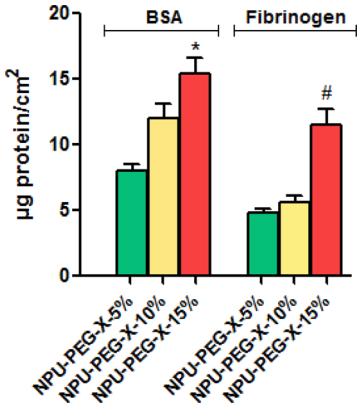

Figure 10. Protein adsorption (BSA and fibrinogen) amounts of NPU-PEG-Xs. * Significantly different from NPU-PEG-X-15% vs NPU-PEG-X-5%, ($p < 0.05$). # Significantly different from NPU-PEG-X-15% vs NPU-PEG-X-10% and NPU-PEG-X-5%, ($p < 0.05$).

adsorption amounts of NPU-PEG-Xs were very similar to these polymers.[36]

Fibrinogen is an important protein which works in blood clotting mechanism. Therefore, fibrinogen adsorption studies have an importance in terms of the interactions between blood and biomaterials. Figure 10 also shows the results of fibrinogen adsorption on PU surfaces. The amounts of adsorbed fibrinogen were 4.81 ± 0.69, 5.67 ± 1.21 and 11.57 ± 2.76 $\mu g/cm^2$ for NPU-PEG-X-5%, NPU-PEG-X-10% and NPU-PEG-X-15%, respectively. These results were slightly high compared to other polymers.[36] According to the results, fibrinogen adsorption is increased with increasing xylose ratio in PUs. The underlying fact caused in increasing of branches in the polymer is related to the increase of xylose ratios. The porous polymer structure is formed and thus amount of adsorbed protein is increased in PUs like BSA adsorption.

Figure 11A shows the relationship between water contact angle and BSA adsorption on the PUs. BSA adsorption on NPU-PEG-X-5%, the most hydrophilic surface, was smaller than moderately hydrophilic surface of NPU-PEG-X-15%. Tsukagoshi et al. examined the relationship between surface wettability and protein adsorption for pMEMA, pHEMA, pAAm, pMMA and pSt polymers. As parallel with our result, they were found that high hydrophobicity caused with high protein adsorption.[36,37] Figure 11B shows the relationship between water contact angle and fibrinogen adsorption on the PUs. The adsorption was the least amount for the most hydrophilic surface, NPU-PEG-X-5%. These findings are consistent with the literature.[6,36]

Cytotoxicity Properties. A common concern in developing a biodegradable biomaterial for tissue applications is the cytotoxic effect of degradation products. Structure and properties of degradation products release from the polymer to medium have an important role in term of biocompatibility of polymer. Therefore, selection of monomers in the PUs structure is very significant for biocompatibility.

It is one hypothesis of this study that xylose containing nonaromatic PUs yield biocompatible adhesives and may help overcome known compatibility problems of PUs which are synthesized with aromatic isocyanetes. We carried out indirect cytocompatibility test of NPU-PEG-Xs with a standard LIVE/DEAD assay on RAOEC endothelial cells.[38] The reduction of cell viability by more than 30% is considered as a cytotoxic effect for biomaterials according to ISO-10993-5.[8] NPU-PEG-X

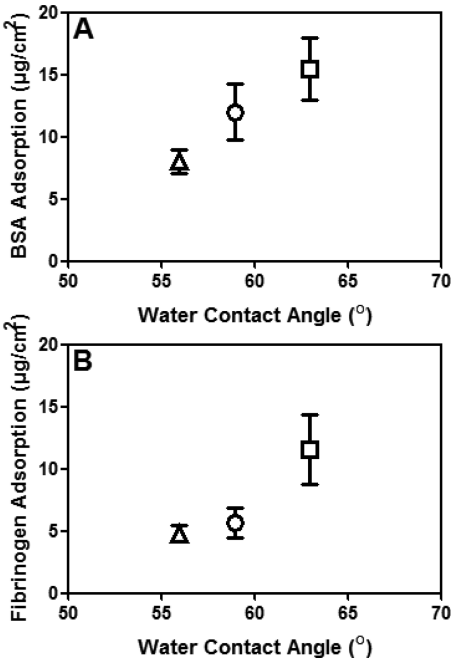

Figure 11. Relationship of water contact angle on NPU-PEG-Xs with BSA adsorption (A) and fibrinogen adsorption (B) for NPU-PEG-X-5% (△), NPU-PEG-X-10% (○) and NPU-PEG-X-15% (□).

samples showed high cell viability (>86%) (Figure 12). These results were also evaluated as grade 1 according to ISO-10993-5 and were revealed that synthesized NPU-PEG-X adhesives can be assumed nontoxic.

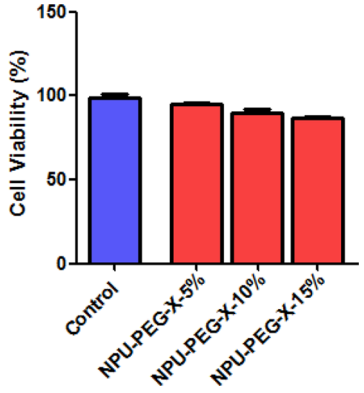

Figure 12. Cell viability results of NPU-PEG-X extracts on RAOEC cell line.

***In Vivo* Biocompatibility Properties.** NPU-PEG-X-10% was selected for *in vivo* biocompatibility as acute (1 week) and chronic (6 weeks) applications taking into consideration of adhesion strength and cytotoxicity tests. Each polyurethane film was placed on the back of the rat in similar sizes (Figure 13). At the end of the implantation period, muscle tissue around the sample in the animals was taken and it was subjected to histological and biochemical examination.

Histological Assessment. In histological analysis, a 0−3 score was used by evaluating neutrophil infiltration, lymphocyte infiltration, macrophage infiltration, mast cell density and collagen density in the connective tissues. They were grouped as Score 0: normal, Score 1: mild (0−25% damage), Score 2:

DOI: 10.1021/acsami.5b12279
ACS Appl. Mater. Interfaces 2016, 8, 4456−4466

Figure 13. *In vivo* appearance of NPU-PEG-X-10% 1 (A) and 6 (B) weeks after implantation.

moderate (25−75% damage), Score 3: severe (>75% damage).[18]

To determine the inflammation that occurs after acute and chronic application of NPU-PEG-X-10% hematoxylin-eosin staining method was applied in the sections (Figure S2). Neutrophil infiltration scores were identified as 0.05 ± 0.02 for 1 week and 0.06 ± 0.02 for 6 weeks in the control group and 0.26 ± 0.52 for 1 week and 0.05 ± 0.02 for 6 weeks in the NPU-PEG-X-10% group (Table 2). By considering the results

Table 2. Histological Findings of Muscle Tissues Following 1 and 6 weeks of NPU-PEG-X-10% Implantation

Histological Evaluation		Scores	
	groups	1 week	6 weeks
neutrophil infiltration	control (PP)	0.05 ± 0.02	0.06 ± 0.02
	NPU-PEG-X-10%	0.26 ± 0.52	0.05 ± 0.02
lymphocyte infiltration	control (PP)	0.06 ± 0.27	0.05 ± 0.02
	NPU-PEG-X-10%	0.46 ± 0.09	0.27 ± 0.05
macrophage infiltration	control (PP)	0.07 ± 0.29	0.08 ± 0.03
	NPU-PEG-X-10%	0.17 ± 0.42	0.17 ± 0.42
mast cell density	control (PP)	0.13 ± 0.03	0.16 ± 0.04
	NPU-PEG-X-10%	0.40 ± 0.05	0.40 ± 0.05
collagen density	control (PP)	0.07 ± 0.02	0.13 ± 0.38
	NPU-PEG-X-10%	0.25 ± 0.51	0.15 ± 0.40

scores for all groups were less than 1, so these results indicate a mild inflammation histologically. Furthermore, in chronic application scores were less than 0.5 and this indicates that neutrophil infiltration developed around 10% of the section in NPU-PEG-X-10% group. These results revealed that inflammation were scarcely observed in NPU-PEG-X-10%.

To determine the inflammation that occurs after acute and chronic application of NPU-PEG-X-10%, sections were applied hematoxylin-eosin staining (Figure S3). Lymphocyte infiltrations were identified as 0.06 ± 0.27 for 1 week and 0.05 ± 0.02 for 6 weeks in the control group and 0.46 ± 0.09 for 1 week and 0.27 ± 0.05 for 6 weeks in the NPU-PEG-X-10% group (Table 2). For the 1 and 6 weeks of the treatment groups, scores were also less than 0.5 as in lymphocyte infiltration. The infiltration of lymphocyte samples for the 6 weeks was determined at the control level. Decreasing in the inflammation and approaching the control values in the chronic period are very important in terms of the applicability of the biodegradable material.

In sections that were applied PAS staining method (Figure S4) during acute and chronic periods macrophage infiltrations were determined as 0.07 ± 0.29 for 1 week and 0.08 ± 0.03 for 6 weeks in the control groups and 0.17 ± 0.42 for both 1 and 6 weeks in NPU-PEG-X-10%.

Mast cells were stained as red in sections which were applied methyl-green proline staining method (Figure S5). Mast cell densities were 0.13 ± 0.03, 0.16 ± 0.04 in the control group and 0.40 ± 0.05, 0.40 ± 0.05 in the NPU-PEG-X-10% group for 1 and 6 weeks, respectively.

In sections which were applied Masson's trichrome staining method (Figure S6) densities of the collagen were determined as 0.07 ± 0.02 and 0.13 ± 0.38 in the control group and 0.25 ± 0.51 and 0.15 ± 0.40 in NPU-PEG-X-10% for 1 and 6 weeks, respectively.

Host reactions following implantation of biomaterials first consist of blood-material interactions and acute inflammation.[39] The acute reaction is determined at the histological level by the presence of polymorphonuclear leukocytes and macrophages, and generally resolves within 1 week.[40,41] However, if the material persists in the tissue, the acute inflammation transforms chronic. The number of polymorphs may decrease and the presence of lymphocytes becomes more prominent, together with macrophages present at the implant surface.[39] In this study, a comparison of the NPU-PEG-X group with the control group, showed a significant increase in lymphocyte and neutrophil infiltration by the first week, but the inflammation was not severe. However, in terms of accumulation inflammatory cells on the sixth week NPU-PEG-X group showed more decline in the inflammation. We postulate that inflammation may be reduced due to tissue regeneration.

Biochemical Evaluation. Biochemical point of view in terms of important indicators of inflammation, myeloperoxidase (MPO) and nitric oxide (NO) levels were determined during acute and chronic periods in tissue samples which were taken from the material. MPO and NO levels in tissues were given in Table 3. MPO was performed in order to analyze inflammatory

Table 3. Biochemical Results of Muscle Tissues Following 1 and 6 weeks of NPU-PEG-X-10% Implantation

	MPO (U/g wet tissue)		NO (nmol/g tissue)	
groups	1 week	6 weeks	1 week	6 weeks
control (PP)	86.6 ± 27.9	114.8 ± 42.3	19.0 ± 2.9	26.1 ± 2.6
NPU-PEG-X-10%	92.7 ± 27.1	93.1 ± 30.4	24.9 ± 3.0	33.4 ± 3.5

cell infiltration into the implanted NPU-PEG-X. MPO, an enzyme derived from activated neutrophils and lymphocyte, is concerned in the production of reactive oxygen species and nitric oxide-based oxidation.[42] In regards to the MPO levels, although there was an increase in 1 week samples compared to the control group, there was no statistically significant difference ($p > 0.05$). MPO levels are particularly associated with the neutrophils and lymphocyte infiltration and according to our studies the both results were quite parallel each other. For 6 weeks samples, MPO levels were close or less than control group and these results were parallel with histological inflammation parameters. According to the MPO results, rat tissues were not shown any inflammatory response against NPU-PEG-X-10%.

As another important inflammation parameter, NO levels were determined in tissue samples and results were given in Table 3. NO produced by activated macrophages is an important effector molecule in the inflammation to foreign materials. Our results are consistent with both histological

DOI: 10.1021/acsami.5b12279
ACS Appl. Mater. Interfaces 2016, 8, 4456−4466

parameters and MPO activity. There was no significant difference between the control and NPU-PEG-X-10% groups ($p > 0.05$). Furthermore, it is known that NO has an important role in regulating inflammatory responses via mast cells. In this respect, analogy between NO levels and mast cell density is important.

CONCLUSION

We described an injectable tissue adhesive polyurethane based on xylose, PEG200 and 4,4′-methylenebis(cyclohexyl isocyanate). The adhesion strengths of 15% xylose containing PUs were measured with Lap-Shear test as 415.0 ± 48.8 and 94.0 ± 2.8 kPa for aluminum substrate and muscle tissue, respectively. Adhesive properties of PUs increased depending on the xylose ratio of NPU-PEG-X. This adhesion result is higher than commercial tissue adhesives used in body. In addition, the biodegradation range of synthesized polyurethanes was 10−20% for 8 weeks of incubation. From indirect cytocompatibility test of NPU-PEG-Xs, biocompatibilities were also evaluated as grade 1 according to ISO-10993-5. In addition, NPU-PEG-X-10% exhibited minimal inflammatory response in the *in vivo* biocompatibility test. As a result, tissue adhesive was developed for minimally invasive effect by focusing the novel aliphatic semisynthetic polyurethanes that can be used in the medical field.

ASSOCIATED CONTENT

Supporting Information

The Supporting Information is available free of charge on the ACS Publications website at DOI: 10.1021/acsami.5b12279.

FT-IR spectra of biodegradation, neutrophil infiltration of surrounding tissue, lymphocyte infiltration of surrounding tissue, macrophage infiltration of surrounding tissue, mast cell density of surrounding tissue, and collagen densities of the surrounding tissues (PDF).

AUTHOR INFORMATION

Corresponding Author

*Burhan Ates. Phone: 90-422 377 3888. Fax: 90-422 341 0037. Email: burhan.ates@inonu.edu.tr.

Notes

The authors declare no competing financial interest.

ACKNOWLEDGMENTS

This study was supported by the grants to B. Ates from The Scientific and Technical Research Council of Turkey (TUBITAK-TBAG-111T104).

REFERENCES

(1) Bouten, P. J. M.; Zonjee, M.; Bender, J.; Yauw, S. T. K.; van Goor, H.; van Hest, J. C. M.; Hoogenboom, R. The Chemistry of Tissue Adhesive Materials. *Prog. Polym. Sci.* **2014**, *39*, 1375−1405.

(2) Ferreira, P.; Silva, A. F. M.; Pinto, M. I.; Gil, M. H. Development of A Biodegradable Bioadhesive Containing Urethane Groups. *J. Mater. Sci.: Mater. Med.* **2008**, *19*, 111−120.

(3) Tajirian, A. L.; Goldberg, D. J. A Review of Sutures and Other Skin Closure Materials. *J. Cosmet. Laser. Ther.* **2010**, *12*, 296−302.

(4) Duarte, A. P.; Coelho, J. F.; Bordado, J. C.; Cidade, M. T.; Gil, M. H. Surgical Adhesives: Systematic Review of The Main Types and Development Forecast. *Prog. Polym. Sci.* **2012**, *37*, 1031−1050.

(5) Reece, T. B.; Maxey, T. S.; Kron, I. L. A Prospectus on Tissue Adhesives. *Am. J. Surg.* **2001**, *182*, S40−S44.

(6) Ferreira, P.; Pereira, R.; Coelho, J. F. J.; Silva, A. F. M.; Gil, M. H. Modification of The Biopolymer Castor Oil with Free Isocyanate Groups To Be Applied As Bioadhesive. *Int. J. Biol. Macromol.* **2007**, *40*, 144−152.

(7) Ninan, L.; Monahan, J.; Stroshine, R. L.; Wilker, J. J.; Shi, R. Adhesives Strength of Marine Mussel Extracts on Porcine Skin. *Biomaterials* **2003**, *24*, 4091−4099.

(8) Liu, Y.; Meng, H.; Konst, S.; Sarmiento, R.; Rajachar, R.; Lee, B. P. Injectable Dopamine-Modified Poly(ethylene glycol) Nanocomposite Hydrogel with Enhanced Adhesive Property and Bioactivity. *ACS Appl. Mater. Interfaces* **2014**, *6*, 16982−16992.

(9) Ates, B.; Koytepe, S.; Karaaslan, M. G.; Balcioglu, S.; Gulgen, S.; Demirbilek, M.; Denkbas, E. B. Chlorogenic Acid Containing Bioinspired Polyurethanes: Biodegradable Medical Adhesive Materials. *Int. J. Polym. Mater.* **2015**, *64*, 611−619.

(10) Peng, Z.; Chen, F. Synthesis and Properties of Lignin-Based Polyurethane Hydrogels. *Int. J. Polym. Mater.* **2011**, *60*, 674−683.

(11) Hill, A.; Estridge, T. D.; Maroney, M.; Monnet, E.; Egbert, B.; Cruise, G.; Coker, G. T. Treatment of Suture Line Bleeding With A Novel Synthetic Surgical Sealant In A Canine Iliac PTFE Graft Model. *J. Biomed. Mater. Res.* **2001**, *58*, 308−312.

(12) Heiss, C.; Kraus, R.; Schluckebier, D.; Stiller, A. C.; Wenisch, S.; Schnettler, R. Bone Adhesives In Trauma and Orthopedic Surgery. *Eur. J. Trauma. Emerg. Surg.* **2006**, *32*, 141−148.

(13) Bilic, G.; Brubaker, C.; Messersmith, P. B.; Mallik, A. S.; Quinn, T. M.; Haller, C.; Done, E.; Gucciardo, L.; Zeisberger, S. M.; Zimmermann, R.; Deprest, J.; Zisch, A. H. Injectable Candidate Sealants For Fetal Membrane Repair: Bonding and Toxicity. *Am. J. Obstet. Gynecol.* **2010**, *202*, 85.e1−85.e9.

(14) Mahdavi, A.; Ferreira, L.; Sundback, C.; Nichol, J. W.; Chan, E. P.; Carter, D. J. D.; Bettinger, C. J.; Patanavanich, S.; Chignozha, L.; Joseph, E. B.; Galakatos, A.; Pryor, H.; Pomerantseva, I.; Masiakos, P. T.; Faquin, W.; Zumbuehl, A.; Hong, S.; Borenstein, J.; Vacanti, J.; Langer, R.; Karp, J. M. A Biodegradable and Biocompatible Gecko-Inspired Tissue Adhesive. *Proc. Natl. Acad. Sci. U. S. A.* **2008**, *105*, 2307−2312.

(15) Ferreira, P.; Coelho, J. F. J.; Gil, M. H. Development of A New Photocrosslinkable Biodegradable Bioadhesive. *Int. J. Pharm. (Amsterdam, Neth.)* **2008**, *352*, 172−181.

(16) Lu, Y.; Tighzert, L.; Dole, P.; Erre, D. Preparation and Properties of Starch Thermoplastics Modified With Waterborne Polyurethane From Renewable Resources. *Polymer* **2005**, *46*, 9863−9870.

(17) Hazer, D. B.; Hazer, B.; Dincer, N. Soft Tissue Response to the Presence of Polypropylene-G-Poly(ethylene glycol) Comb-Type Graft Copolymers Containing Gold Nanoparticles. *J. Biomed. Biotechnol.* **2011**, *2011*, 1−7.

(18) Tasdemir, S.; Tasedmir, C.; Vardi, N.; Ates, B.; Taslidere, E.; Karaaslan, M. G.; Sapmaz, H. I.; Sagir, M.; Kurt, A.; Baser, C. A. Effects of Ozone Therapy on Cyclophosphamide-induced Urinary Bladder Toxicity in Rats. *Clin. Invest. Med.* **2013**, *36*, E9−E17.

(19) Kizuka, K.; Inoue, S. I. Synthesis and Properties of Polyurethane Elastomers Containing Sucrose as a Cross-Linker. *Open J. Org. Polym. Mater.* **2015**, *5*, 103−112.

(20) Mehdizadeh, M.; Yang, J. Design Strategies and Applications of Tissue Bioadhesives. *Macromol. Biosci.* **2013**, *13*, 271−288.

(21) Sirkecioglu, A.; Mutlu, H. B.; Citak, C.; Koc, A.; Guner, F. S. Physical and Surface Properties of Polyurethane Hydrogels in Relation with Their Chemical Structure. *Polym. Eng. Sci.* **2014**, *54*, 1182−1191.

(22) Sheikh, N.; Mirzadeh, H.; Katbab, A. A.; Salehian, P.; Daliri, M.; Amanpour, S. Isocyanate-Terminated Urethane Prepolymer as Bioadhesive Material: Evaluation of Bioadhesion and Biocompatibility, *In Vitro* and *In Vivo* Assays. *J. Biomater. Sci., Polym. Ed.* **2001**, *12*, 707−719.

(23) Meredith, H. J.; Jenkins, C. L.; Wilker, J. J. Enhancing the Adhesion of a Biomimetic Polymer Yields Performance Rivaling Commercial Glues. *Adv. Funct. Mater.* **2014**, *24*, 3259−3267.

DOI: 10.1021/acsami.5b12279
ACS Appl. Mater. Interfaces 2016, 8, 4456−4466

(24) Jenkins, C. L.; Meredith, H. J.; Wilker, J. J. Molecular Weight Effects upon the Adhesive Bonding of a Mussel Mimetic Polymer. *ACS Appl. Mater. Interfaces* **2013**, *5*, 5091−5096.
(25) Pérez, C. R. M.; White, J. D.; Wilker, J. J. Polymer Composition and Substrate Influences on the Adhesive Bonding of a Biomimetic, Cross-Linking Polymer. *J. Am. Chem. Soc.* **2012**, *134*, 9498−9505.
(26) Monahan, J.; Wilker, J. J. Cross-Linking the Protein Precursor of Marine Mussel Adhesives: Bulk Measurements and Reagents for Curing. *Langmuir* **2004**, *20*, 3724−3729.
(27) Alberts, E. M.; Taylor, S. D.; Edwards, S. L.; Sherman, D. M.; Huang, C. P.; Kenny, P.; Wilker, J. J. Structural and Compositional Characterization of the Adhesive Produced by Reef Building Oysters. *ACS Appl. Mater. Interfaces* **2015**, *7*, 8533−8538.
(28) Murakami, Y.; Yokoyama, M.; Okano, T.; Nishida, H.; Tomizawa, Y.; Endo, M.; Kurosawa, H. A Novel Synthetic Tissue-Adhesive Hydrogel Using a Crosslinkable Polymeric Micelle. *J. Biomed. Mater. Res., Part A* **2007**, *80* (2), 421−427.
(29) Mehdizadeh, M.; Weng, H.; Gyawali, D.; Tang, L.; Yang, J. Injectable Citrate-Based Mussel-Inspired Tissue Bioadhesives with High Wet Strength for Sutureless Wound Closure. *Biomaterials* **2012**, *33*, 7972−7983.
(30) Sierra, D. H. Fibrin Sealant Adhesive Systems: A Review of Their Chemistry, Material Properties And Clinical Applications. *J. Biomater. Appl.* **1993**, *7*, 309−352.
(31) McDermott, M. K.; Chen, T.; Williams, C. M.; Markley, K. M.; Payne, G. F. Mechanical Properties of Biomimetic Tissue Adhesive Based on the Microbial Transglutaminase-Catalyzed Crosslinking of Gelatin. *Biomacromolecules* **2004**, *5*, 1270−1279.
(32) Ishihara, M.; Nakanishi, K.; Ono, K.; Sato, M.; Kikuchi, M.; Saito, Y.; Yura, H.; Matsui, T.; Hattori, H.; Uenoyama, M.; Kurita, A. Photocrosslinkable Chitosan as a Dressing for Wound Occlusion and Accelerator in Healing Process. *Biomaterials* **2002**, *23*, 833−840.
(33) Sung, H. W.; Huang, D. M.; Chang, W. H.; Huang, R. N.; Hsu, J. C. Evaluation of Gelatin Hydrogel Crosslinked with Various Crosslinking Agents as Bioadhesives: *In Vitro* Study. *J. Biomed. Mater. Res.* **1999**, *46*, 520−530.
(34) Zhang, M.; He, X.; Chen, L.; Zhang, Y. Preparation of IDA-Cu Functionalized Core−Satellite Fe3O4/polydopamine/Au Magnetic Nanocomposites and Their Application for Depletion of Abundant Protein in Bovine Blood. *J. Mater. Chem.* **2010**, *20*, 10696−10704.
(35) Shi, H.; Tsai, W. B.; Garrison, M. D.; Ferrari, S.; Ratner, B. D. Template-imprinted Nanostructured Surfaces for Protein Recognition. *Nature* **1999**, *398*, 593−597.
(36) Tsukagoshi, T.; Kondo, Y.; Yoshino, N. Protein Adsorption on Polymer-Modified Silica Particle Surface. *Colloids Surf., B* **2007**, *54*, 101−107.
(37) Changsheng, Z.; Xiangdong, L.; Motoyoshi, N.; Norio, N. Blood Compatible Aspects of DNA-Modified Polysulfone Membrane—Protein Adsorption and Platelet Adhesion. *Biomaterials* **2003**, *24*, 3747−3755.
(38) Loth, T.; Hötzel, R.; Kascholke, C.; Anderegg, U.; Siegmund, M. S.; Hacker, M. C. Gelatin-Based Biomaterial Engineering with Anhydride-Containing Oligomeric Cross-Linkers. *Biomacromolecules* **2014**, *15*, 2104−2118.
(39) Anderson, J. M.; Rodriguez, A.; Chang, D. T. Foreign Body Reaction to Biomaterials. *Semin. Immunol.* **2008**, *20*, 86−100.
(40) Qu, X. H.; Wu, Q.; Zhang, K. Y.; Chen, G. Q. *In Vivo* Studies of Poly(3-Hydroxybutyrate-co-3-Hydroxyhexanoate) Based Polymers: Biodegradation and Tissue Reactions. *Biomaterials* **2006**, *27*, 3540−3548.
(41) Baykal, A.; Onat, D.; Rasa, K.; Renda, N.; Sayek, I. Effects of Polyglycolic Acid and Polypropylene Meshes on Postoperative Adhesion Formation in Mice. *World J. Surg.* **1997**, *21*, 579−583.
(42) Laschke, M. W.; Strohe, A.; Scheuer, C.; Eglin, D.; Verrier, S.; Alini, M.; Pohlemann, T.; Menger, M. D. In Vivo Biocompatibility and Vascularization of Biodegradable Porous Polyurethane Scaffolds for Tissue Engineering. *Acta Biomater.* **2009**, *5*, 1991−2001.

DOI: 10.1021/acsami.5b12279
ACS Appl. Mater. Interfaces 2016, 8, 4456−4466